

RESEARCH

Open Access



# A glutamine metabolish-associated prognostic model to predict prognosis and therapeutic responses of hepatocellular carcinoma

Hao Xu<sup>1</sup>, Hui Pan<sup>2</sup>, Lian Fang<sup>3</sup>, Cangyuan Zhang<sup>4,5\*</sup>, Chen Xiong<sup>5\*</sup> and Weiti Cai<sup>1\*</sup>

## Abstract

Hepatocellular carcinoma (HCC) ranks among the most lethal malignancies around the world. However, the current management strategies for predicting prognosis in HCC patients remain unreliable. Our study developed a robust prognostic model based on glutamine metabolism associated-genes (GMAGs), utilizing data from The Cancer Genome Atlas database. The prognostic values of model were validated through the databases of the Gene Expression Omnibus and International Cancer Genome Consortium via Kaplan–Meier curves and receiver operating characteristic (ROC). The potential biological pathways associated with prognostic risk were investigated through different enrichment analysis, and Gene variation analysis. The correlation between prognostic model and therapeutic responses were analyzed. Quantitative real-time PCR (qRT-PCR) and cellular experiments were measured to analyze the GMAGs. Consequently, a prognostic model was constructed of 4 GMAGs (RRM1, RRM2, G6PD, and GPX7) through least absolute shrinkage and selection operator (LASSO) regression analysis. The Kaplan–Meier curves and ROC curves showed a reliable predictive capacity of prognosis for HCC patients ( $p < 0.05$ ). The enrichment analyses revealed a multitude of biological pathways that are significantly associated with cancer. Patients with high prognostic risk might be sensitive to immunotherapy ( $p < 0.05$ ). The results of qRT-PCR revealed that all 4 GMAGs exhibited significantly higher expression levels in HCC samples compared to normal samples ( $p < 0.05$ ). Moreover, the knockdown of RRM1 suppresses the progression of HCC cells. In this study, we developed a robust prognostic model for predicting the prognosis of HCC patients based on GMAGs, and identified RRM1 as a potential therapeutic target for HCC.

**Keywords** Glutamine, Metabolism, Hepatocellular carcinoma, Prognostic model

\*Correspondence:

Cangyuan Zhang  
zhangcy156707@foxmail.com

Chen Xiong

xcdmu2024@163.com

Weiti Cai

wtcyyy@163.com

<sup>1</sup>Department of Hepatobiliary Surgery, Siyang Hospital, Suqian, Jiangsu 223799, China

<sup>2</sup>Department of General Surgery, The Second Affiliated Hospital of Nanchang University, Nanchang, Jiangxi 330008, China

<sup>3</sup>Department of Gastrointestinal Surgery, Pingxiang People's Hospital of Jiangxi Province, Pingxiang, Jiangxi 337000, China

<sup>4</sup>Department of Hepatobiliary Surgery, Shandong Public Health Clinical Center, Jinan, Shandong 250013, China

<sup>5</sup>Dalian Medical University, Dalian, Liaoning 116044, China



© The Author(s) 2024. **Open Access** This article is licensed under a Creative Commons Attribution-NonCommercial-NoDerivatives 4.0 International License, which permits any non-commercial use, sharing, distribution and reproduction in any medium or format, as long as you give appropriate credit to the original author(s) and the source, provide a link to the Creative Commons licence, and indicate if you modified the licensed material. You do not have permission under this licence to share adapted material derived from this article or parts of it. The images or other third party material in this article are included in the article's Creative Commons licence, unless indicated otherwise in a credit line to the material. If material is not included in the article's Creative Commons licence and your intended use is not permitted by statutory regulation or exceeds the permitted use, you will need to obtain permission directly from the copyright holder. To view a copy of this licence, visit <http://creativecommons.org/licenses/by-nc-nd/4.0/>.

## Introduction

Globally, hepatocellular carcinoma (HCC) ranks sixth in prevalence and third in tumor-related mortality [1]. At present, radical surgical resection, targeted therapy, liver transplantation represent the optimal therapeutic modalities for liver cancer [2, 3]. Due to the lack of early-stage symptoms and signs, approximately 60% of liver cancer patients are diagnosed at an intermediate or advanced stage, thereby missing the window for early surgical intervention [4, 5]. Hence, it is imperative to identify novel therapeutic targets and enhance prognostic management strategies.

Although glutamine is not an essential amino acid, it assumes a conditionally essential status when catabolic stress occurs, such as after surgery and trauma, the demand for glutamine in the gastrointestinal tract, kidneys, and immune system increases dramatically [6, 7]. In addition, a close relationship exists between glutamine and tumor malignant progression [8]. Due to the rapid proliferation of tumor cells, glutamine is used as a fuel for energy supply of tumor cells and an important precursor for synthesis of nucleotides, proteins and glutathione (GSH) [9]. As a result, the synthesis of glutamine cannot meet the needs of tumor proliferation, and glutamine is transformed into a conditional essential amino acid [10]. Rapidly proliferating tumor cells have a greater demand for glutamine. The involvement of glutamine in the progression of liver cancer has been extensively demonstrated [11–13], highlighting its potential as a prognostic indicator and therapeutic target for this disease. Therefore, targeting each step of glutamine metabolism is pivotal in identifying drug targets and developing anti-tumor medications.

The present study utilized the ICGC and TCGA databases to identify four glutamine metabolism-associated genes (GMAGs). In the following, we examined the correlation between clinical characteristics and the expression levels of these genes. Furthermore, a prognostic nomogram was constructed based on these genes, some cellular experiments about RRM1 genes were executed to illustrate the oncogenic roles of RRM1 in HCC, indicating that RRM1 represents a promising therapeutic target for HCC.

## Materials and methods

### Data sources and samples collection

A cohort comprising HCC samples and paracancerous samples from 374 patients, along with corresponding clinical information and FPKM data of mRNA, was obtained from TCGA-LIHC dataset in The Cancer Genome Atlas (TCGA) database (<https://portal.gdc.cancer.gov/>) [14]. Besides, the clinical and mRNA data of another cohort contained data of 243 HCC samples and 202 paracancerous samples from the International

Cancer Genome Consortium (ICGC) database (<https://dcc.icgc.org/projects/LIRI-JP>) [15]. Another data of validation cohort that contained 225 HCC samples and 220 normal liver samples were acquired from the GSE14520 dataset in Gene Expression Omnibus (GEO) database (<https://www.ncbi.nlm.nih.gov/geo>) [16]. All raw data from TCGA, ICGC, and GEO databases were collated to matrixes by Perl language (<https://www.perl.org>). 50 glutamine metabolism-associated genes (GMAGs) were obtained from the Human Gene Set (GOBP\_Glutamine\_Metabolic\_Process) in the Gene Set Enrichment Analysis (GSEA) online database ([https://www.gsea-msi.gdb.org/gsea/msigdb/human/geneset/GOBP\\_GLUTAMINE\\_METABOLIC\\_PROCESS.html](https://www.gsea-msi.gdb.org/gsea/msigdb/human/geneset/GOBP_GLUTAMINE_METABOLIC_PROCESS.html)). Data of therapeutic responses to sorafenib and transhepatic arterial chemotherapy and embolization (TACE) were downloaded from GSE109211 and GSE104580 datasets. Data about immune landscape and genomic mutations were also gained from TCGA database. Clinical samples of HCC patients were acquired from Dalian medical university, the Department of hepatobiliary surgery, Shandong Public Health Clinical Center, and the Department of hepatobiliary surgery, Siyang Hospital. All experiments based on clinical sampled were approved by the Ethics Committee of Dalian medical university. Before the surgery, each patient had signed the informed consent for this study.

### Establishing the prognostic model based on GMAGs

At first, we identified the differentially expressed glutamine metabolism associated-genes (DEGMAGs) between para-tumor and tumor samples by mRNA data from TCGA database via “limma” package through R 4.3.1 software (<https://www.r-project.org/>) ( $|\log_2FC| > 1$  and  $p < 0.05$ ). In order to identify prognostic DEGMAGs, we utilized the univariate Cox regression analysis based on the “survminer” and “survival” packages. The “survival” and “glmnet” packages were performed to achieve LASSO (least absolute shrinkage and selection operator) regression analysis. Through choosing the optimal penalty parameter  $\lambda$  value associated with the minimum 10-fold cross validation, 4 GMAGs were identified to build prognostic model after the LASSO regression analysis. The formula of the prognostic model is that: risk score =  $\sum$  (expression of gene  $i$  \* coefficient gene  $i$ ). According to the expression of 4 GMAGs, each HCC patients might have their own risk score based on this prognostic model. In this formula, corresponding coefficient of 4 GMAGs were showed in Table 1.

### Validating the predictive capacity of a prognostic model

All patients were divided into different groups based on the median value of their risk scores. According to the clinical prognostic data from TCGA database, the

**Table 1** The coefficients of 4 GMAGs in the prognostic model

Gene	Coef
G6PD	0.273363187072334
GPX7	0.00469397166791365
RRM1	0.111586612139908
RRM2	0.0482527705709431

receiver operating characteristic (ROC) curves, the scatterplots, and Kaplan–Meier (K–M) curves were plotted by the “survminer”, “survival”, and “pheatmap” packages to assess the prognostic predictive value of this prognostic model. The prognostic survival curves of 4 GMAGs were plotted through Gene Expression Profiling Interactive Analysis (GEPIA) website (<http://gepia.cancer-pku.cn/index.html>). Besides, the Cox regression analyses including age, gender, grade, TNM stage were also performed to validate the prognostic value of riskscore.

Patients from GSE14520 dataset and ICGC database were also divided into different groups according to the median value of riskscores. The scatterplots, K–M curves, and ROC curves were also plotted to further illustrate the potential prognostic value of this prognostic model.

#### Analyzing the correlation between the clinical features and prognostic model

Stratified analyses of clinicopathological features were used to divide HCC patients into different risk groups in order to further explore the prognostic value of prognostic models. The “limma” package was employed to compare the risk scores among patients exhibiting diverse clinical features. Additionally, the K–M curves were also plotted to further explore the value of prognostic model under the stratified analyzes.

#### Biological functions enrichment analyzes

To investigate the possible biological signaling pathways and functions associated with this prognostic model, “limma” package were utilize to acquire the differentially expressed genes (DEGs) between HCC samples with different prognostic risks. Enrichment analyses based on the DAVID website (<http://david.abcc.ncifcrf.gov/>) were conducted for Kyoto Encyclopedia of Genes and Genomes (KEGG) and Gene Ontology (GO). In addition, enrichment analyses of GSEA (Gene Set Variation Analysis) and GSEA were also performed by “limma”, “GSEABase”, “GSEA” packages to find potential biological signaling pathways and functions.

#### Establishing a prognostic nomogram

A nomogram based on the prognostic model was established via the data of TCGA-LIHC dataset via “Formula”, “foreign”, “lattice”, “Hmisc”, “rms”, and “ggplot2” packages. The corresponding calibration plots and ROC curves were plotted to validate the reliability of this nomogram.

In addition, the Cox regression analyses were also used to further the prognostic value of the nomogram.

#### Assessing the therapeutic responses via prognostic model

To investigate the association between prognostic model and therapeutic responses of HCC patients. Data from GSE104580 and GSE109211 were analyzed to assess the therapeutic responses to TACE (Transhepatic Arterial Chemotherapy and Embolization) and sorafenib, respectively. The Tumor Immune Dysfunction and Exclusion (TIDE) scores were analyzed to compare the immunotherapeutic responses. Patients with higher TIDE scores usually have worse immunotherapeutic responses. Besides, the expression of PDCD1, LAG3, CTLA4, and HAVCR2 in TCGA-LIHC dataset were also analyze to compare the immunotherapeutic responses of patients with different prognostic risks. As we all know, patients with high expression of these immune checkpoint genes might be more sensitive to immunotherapy.

Furthermore, the association between the prognostic model and commonly used chemotherapeutic agents for tumors was assessed using the “oncoPredict” package in R software.

#### Quantitative real-time PCR (qRT-PCR)

Total RNA of tissues was isolated by the Trizol reagent (Yeasen, Shanghai, China). Reverse transcription was performed to acquire cDNA by using a HiScript II Q Select RT SuperMix for qPCR (Vazyme, Nanjing, China). Besides, qRT-PCR was performed by ChamQ SYBR qPCR Master Mix reagent (Yeasen, Shanghai, China). The  $2^{-\Delta\Delta CT}$  was used to quantify the gene expression.

#### Western blot (WB)

Proteins of cells were isolated by radioimmunoprecipitation assay lysis buffer (Yeasen, Shanghai, China) with  $1\mu\text{M}$  PMSE. The lysates were centrifuged at 13,000 g for 20 min. Samples were added to SDS-PAGE loading buffer. After electrophoresis, the proteins were transferred to a PVDF membrane. Then, the membranes were blocked with 5% nonfat milk powder in Tris-buffered saline-Tween (TBST) for an hour. The membranes were incubated with primary antibody ( $\beta$ -actin, Proteintech, 1:20000; RRM1, Proteintech, 1:1000) at 4 °C. After 12 h, the membranes were incubated with second antibodies for an hour. Finally, the images of WB were acquired by adding the ECL and operating the ChemiDoc XRS+ imager.

#### Cell cultures and transfection

Huh7 and Hep3B cell lines were gained from Shanghai Cell Bank, Chinese Academy of Sciences (Shanghai, China). Cells were cultured in Dulbecco’s modified Eagle’s medium (DMEM, Gibco, USA) that contained penicillin

(100 IU/ml), streptomycin (100 µg/ml), and 10% fetal bovine serum. All cells were cultured in a humidified atmosphere at 37 °C containing 5% CO<sub>2</sub>.

The small interfering RNA (siRNA) in this study were acquired from RiboBio company (Guangzhou, China). According to the specification, all siRNAs were transfected into cells by the lipofectamine 2000 (Vazyme, Nanjing, China).

### Cell proliferative assays

Using an Edu (5-ethynyl-20-deoxyuridine) assay kit (Beyotime, Shanghai, China), we evaluated the proliferation of Huh7 cells using the EdU incorporation assay. Huh7 cells were seeded in 6-well-plates at 4×10<sup>5</sup> cells/well for 18 h. 10 µM Edu reagent was added to 6 wells and incubated for 4 h at 37 °C. All figures were gained by using a fluorescence microscope (LEICA, Germany). Finally, the rates of Edu positive cells were calculated.

Cell-Counting-Kit-8 (CCK8) was also used to assess cell proliferation. HCC cells transfected with siRNA were seeded in 96-well-plate at 4×10<sup>3</sup> cells/well. 10 µM CCK8 reagent was added to each well and incubated for an hour at 37 °C. The OD value of each well at 450 nm were measured by a microplate reader.

### Cell migration and invasion assays

A 24-well plate with or without matrigel was seeded with cells transfected with siRNA or negative control vector for comparing their migration and invasion capabilities. 5×10<sup>4</sup> cells were seeded in the upper Transwell chambers without serum. 650 µl DMEM medium with double concentration of serum were added into the 24-well plate. The cells were fixed to the lower chambers by methanol for 30 min. Finally, these fixed cells were dyed by crystal violet solution for 20 min. Images were photographed by microscopes.

Additionally, the wound healing assay was also employed to evaluate the migrative ability of cells. Enough cells were incubated in 6-well plate. Scratches were created by a 200 µl pipette tips. Images were acquired by microscopes from 0 h to 48 h.

### Statistical analysis

R 4.3.1 software was used for all statistical analyses and plotting figures in this study. The results of variation analysis were analyzed via t test.  $P < 0.05$  was deemed to be statistically significant. \* $p$  value  $< 0.05$ ; \*\* $p$  value  $< 0.01$ ; \*\*\* $p$  value  $< 0.001$ .

## Results

### Construction of the prognostic model by GMAGs

According to the analysis of DEGs, 12 GMAGs were identified (Fig. 1A-B). The result of univariate Cox regression analysis indicated that 7 GMAGs might have

independent prognostic values ( $p < 0.05$ ) (Fig. 1C). After performing the LASSO regression analysis, the chosen log ( $\lambda$ ) value is -3.4, which was chosen by the point of minimum error in the cross validation (Fig. 1D). In Fig. 1E, according to the chosen log ( $\lambda$ ) value, coefficients of 4 GMAGs were identified through the Y axis of the intersection of 4 curves and the chosen log ( $\lambda$ ) value. 4 GMAGs and corresponding coefficient were screened and they consisted of the prognostic model (Fig. 1D-E; Table 1).

### Verification of the prognostic model

After dividing HCC patients into low-risk group and high-risk group, the heatmap was showed to exhibit the expression of 4 GMAGs (Fig. 2A). In the scatter plot, patients with higher riskscores might have higher mortality (Fig. 2B-C). The K-M curves showed that patients in the high-expression group have worse OS (overall survival) ( $p < 0.05$ ) and PFS (progression free survival) ( $p = 0.01$ ) rates (Fig. 2D-E). The AUC value of ROC curve to predict 1 year' OS was 0.761 (Fig. 2F). The results of Cox regression analyses showed an independent prognostic predictive capacity of the risk score (Hazard ratio  $> 1$ ,  $p < 0.001$ ) (Fig. 2G-H). Survival curves showed that patients with high expression of 4 GMAGs might have worse prognosis ( $p < 0.05$ ) (Fig. S1).

In the analyses of data from ICGC and GSE14520 datasets, patients were ranked via the value of their risk score, half of HCC patients whose risk score were bigger than the median of risk scores were divided into high-risk group. Other patients were divided into low-risk groups. the scatter plots (Fig. 3A-D) and K-M curves (Fig. 3E-F) also showed a prognostic predictive value of prognostic model. In these results, patients with high-risk scores showed lower survival times and overall survival rates ( $p < 0.05$ ).

### Enrichment analyses correlated with prognostic model

According to the DEGs between HCC patients in different risk groups, potential biological function was explored. The GSVA analysis was showed in Fig. 4A. The results included some metabolic pathways such as fatty acid metabolism, retinol metabolism, and pyruvate metabolism, which hinted that the DEGs might play essential roles in metabolism. GO and KEGG analyses were plotted in Fig. 4B. These results showed some immune functions included leukocyte mediated immunity, immunoglobulin complex, and antigen binding, which reminded that patients with different risk scores might have different immune states. Besides, the results of GSEA analyses about up-regulated and down-regulated DEGs exhibited similar biological pathways with the results of GSVA analysis (Fig. 4C-D).

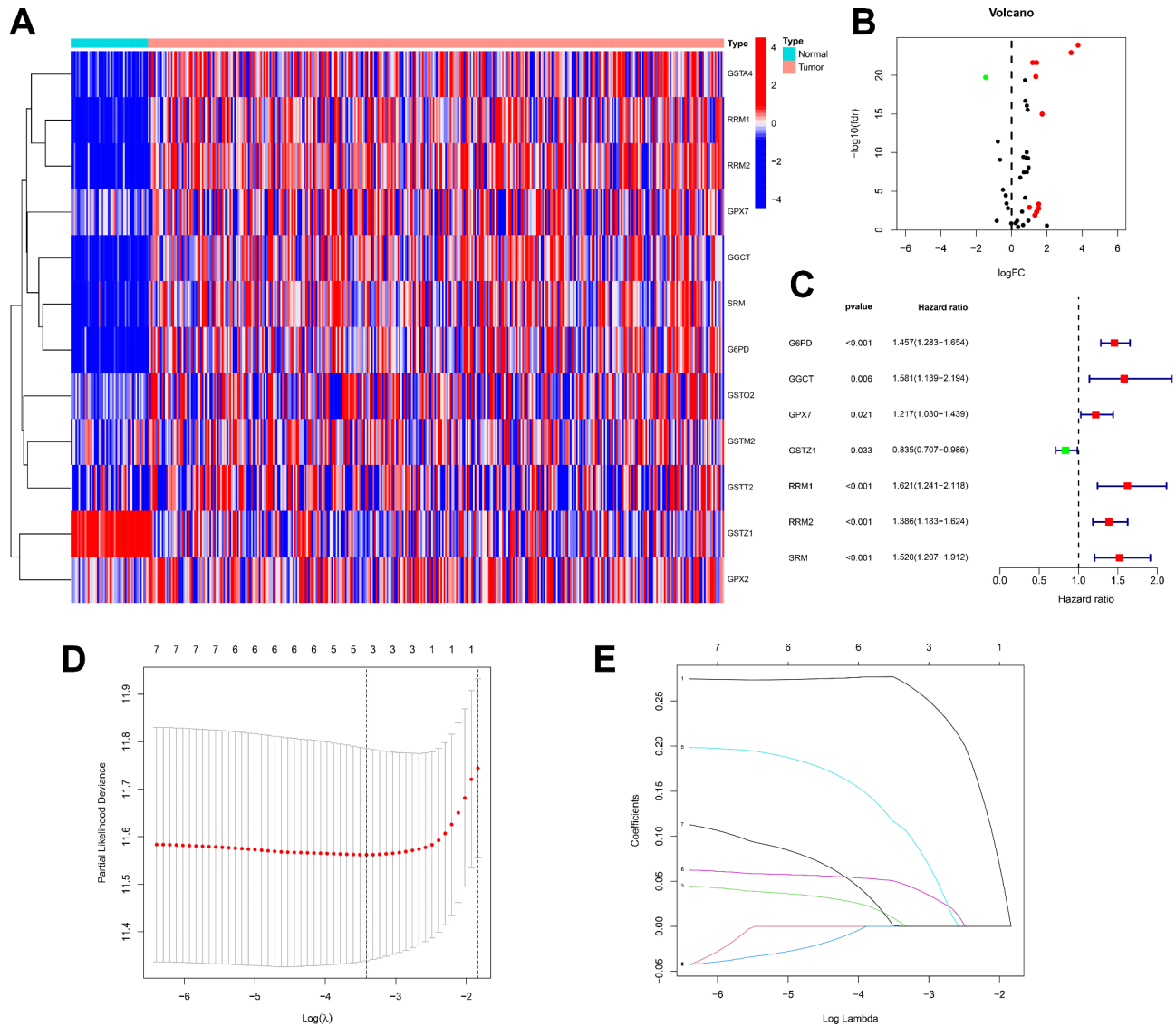


**Fig. 1** Construction of the prognostic model. (A-B) The heatmap and volcano map to show 12 DEGMAGs in TCGA database. (C) The result of univariate Cox regression analysis to identify 7 DEARGs with prognostic values. (D-E) LASSO regression analysis to identify 4 DEARGs that consisted of the prognostic model

**Establishment and validation of prognostic nomogram**

A prognostic nomogram based on clinical features and a prognostic model was developed and showed in Fig. 5A. The corresponding calibration plot showed a strong prognostic predictive capacity of nomogram (Fig. 5B). The ROC curve of the nomogram also showed a wonderful prognostic predictive ability of nomogram (AUC=0.752) (Fig. 5C). The prognostic predictive value of nomogram was further illustrated by the Cox regression analyses between the nomogram and some clinical features (age, gender, grade, stage, T, M, and N) (Hazard ratio > 1,  $p < 0.01$ ) (Fig. 5D-E).

**Assessment of HCC patients’ therapeutic responses via prognostic model**

After dividing HCC patients into different risk groups in GSE104580 and GSE109211 datasets, the risk score of patients were exhibited (Fig. 6A-D). Patients with higher risk scores have lower ratio of therapeutic responses and patients who have therapeutic responses used to have lower risk scores. These results hinted that patients with high prognostic risks might be more insensitive to TACE and sorafenib therapy. Patients with high prognostic risks universally had lower TIDE scores ( $p < 0.05$ ), which meant that these patients might be more sensitive to immunotherapy (Fig. 6E). Furthermore, 4 common immune checkpoint genes were more highly expressed in the high-risk group than in the low-risk group, indicating

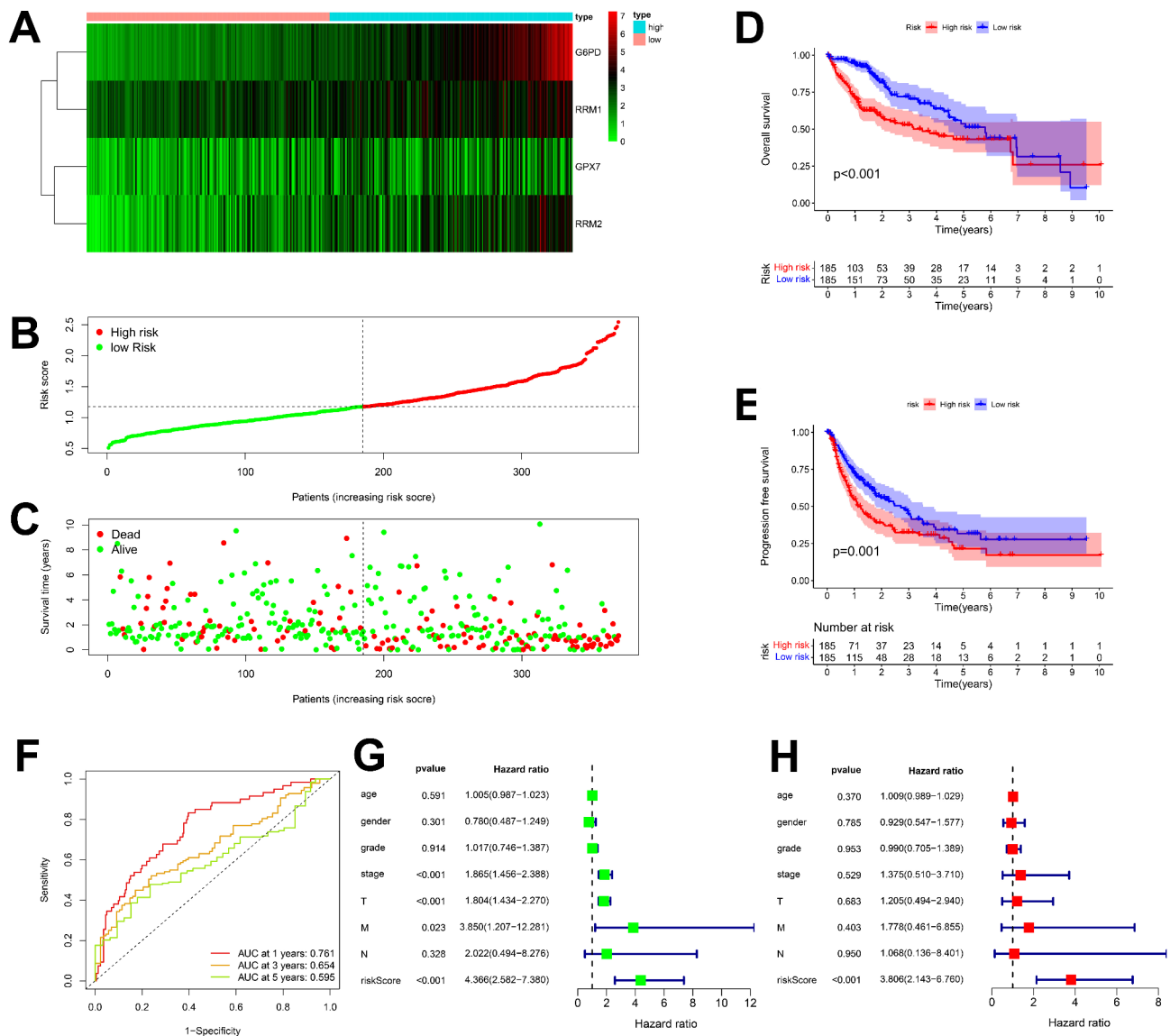


**Fig. 2** Validation of the prognostic model via TCGA database. **(A)** The heatmap to show the expression of 4 DEARs in patients with different prognostic risks. **(B-C)** The scatter plots to show the survival condition of HCC patients. **(D)** K-M curves to showed the OS rates of patients with different prognostic risks. **(E)** K-M curves to showed the PFS rates of patients with different prognostic risks. **(G-H)** The results of univariate and multivariate Cox regression analyses to show an independent prognostic value of the risk score

a potential heightened response to immunotherapy (Fig. 6F).

The therapeutic responses to common chemotherapeutics between patients with different prognostic risks were evaluated via calculating the IC50 value. The most remarkable 8 chemotherapeutics were listed in Fig.S2 ( $p < 0.05$ ).

**Evaluating the expression of 4 GMAGs in HCC tissues**

To assess the differential mRNA expression of GMAGs in HCC, we performed qRT-PCR on 15 paired samples of HCC tissues and their corresponding paracancerous tissues. As shown in Fig. 7, the expression levels of

all four GMAGs were significantly elevated in HCC tissues compared to adjacent non-tumor tissues (RRM1, 1.5-fold,  $p < 0.05$ ; RRM2, 1.5-fold,  $p < 0.001$ ; G6PD, 2-fold,  $p < 0.001$ ; GPX7, 2-fold,  $p < 0.05$ ), suggesting their potential as valuable biomarkers for HCC diagnosis and prognosis. Furthermore, their overexpression highlights their possible roles as therapeutic targets for modulating glutamine metabolism in HCC.

**RRM1 regulate the progression of HCC in vitro**

In 4 GMAGs, the biological functions of RRM1 in HCC had not been explored. We knocked down the expression of RRM1 in Huh7 and Hep3B cells by siRNA. The

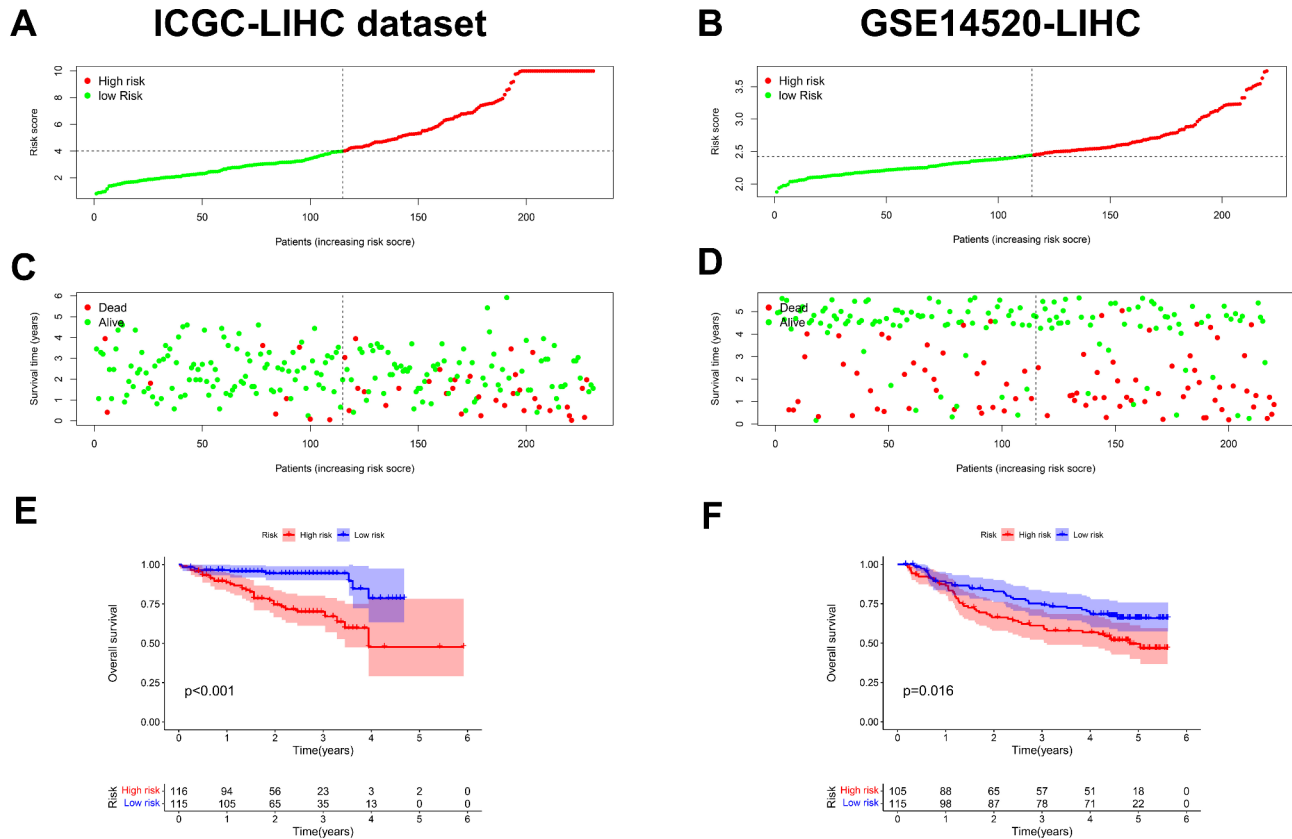


**Fig. 3** Validation of the prognostic model by ICGC and GSE14520 datasets. **(A, C)** The scatter plots to show the survival condition of HCC patients by ICGC database. **(B, D)** The scatter plots to show the survival condition of HCC patients by GSE14520 dataset. **(E)** K-M curves to showed the OS rates of patients with different prognostic risks in ICGC database. **(F)** K-M curves to showed the OS rates of patients with different prognostic risks in GSE14520 dataset

levels of knockdown were demonstrated through qRT-PCR (Fig. 8A) and WB (Fig. 8B). The results showed that siRNA3 was the most effective sequence to knock down the expression of RRM1 in Huh7 and Hep3B cells.

The results of CCK8 assay illustrated that the knockdown of RRM1 could effectively inhibit the proliferation of Huh7 and Hep3B cells ( $p < 0.05$ ) (Fig. 8C). Additionally, the Edu assay was also used to compare the proliferative capacities of Huh7 and Hep3B cells. It was also demonstrated that the knockdown of RRM1 reduced the Edu positive rates of Huh7 and Hep3B cells ( $p < 0.05$ ) (Fig. 8D), which hinted a lower proliferative level of cells with low RRM1 expression. These results illustrated that the knockdown of RRM1 might inhibit the proliferation of HCC.

In addition, the invasion and migration of Huh7 and Hep3B cells could also be regulated by the expression of RRM1. The results of transwell demonstrated that lower expression of RRM1 could significantly inhibit the invasive and migrative capacities of Huh7 and Hep3B cells ( $p < 0.05$ ) (Fig. 8E). Furthermore, the wound healing assay also showed that lower expression of RRM1 could slow down the migrative ability of Huh7 and Hep3B cells ( $p < 0.05$ ) (Fig. 8F).

### Discussion

HCC has become a worldwide healthy problem because of the high morbidity. High glutamine metabolic rate has been demonstrated to be a typical feature of HCC [12, 17, 18]. GMAGs has been illustrated to play pivotal roles in HCC development. Many studies illustrated that GMAGs might have diagnostic values and could be a possible therapeutic target [19–21]. Thus, it might be a possible method to investigate the potential values of GLAS for better diagnosis or treatment of HCC patients.

In this research, we established a prognostic model according to GMAGs and prognostic data sourced from the TCGA database. At first, we acquired 12 GMAGs from GSEA database and identified 4 GMAGs with prognostic values to establish the prognostic model. The prognostic predictive power of this model was demonstrated via K-M curves and ROC curves based on data from TCGA, ICGC, and GEO databases. The enrichment analyses were conducted to investigate potential biological pathways associated with GMAGs. Plenty of biological pathways correlated with cancer such as PPAR or P53 signaling pathway were exhibited in the results, which meant that these GMAGs might play crucial roles in cancers. A prognostic nomogram based on this prognostic

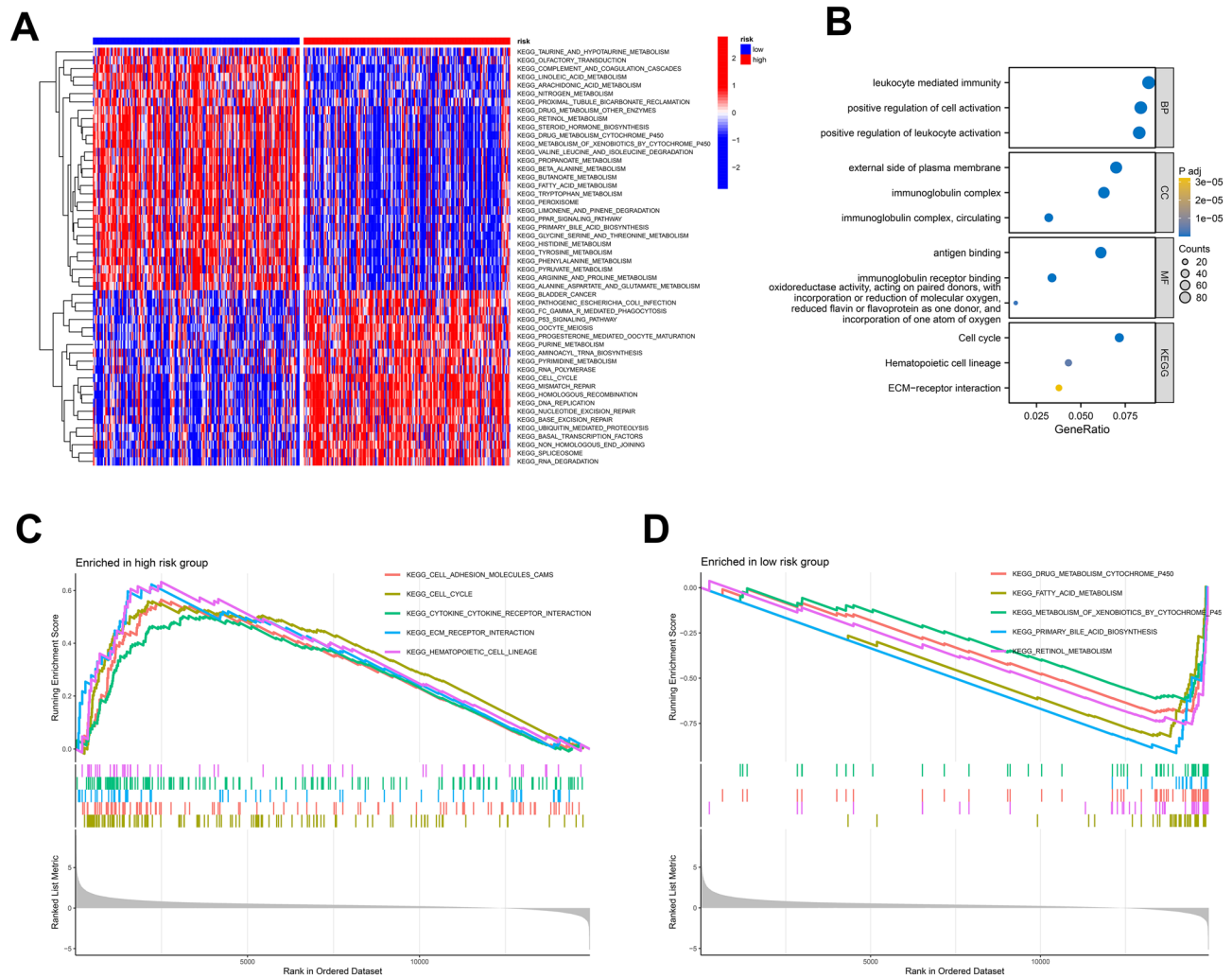


**Fig. 4** Enrichment analyses associated with the prognostic model. **(A)** GSVA analysis. **(B)** GO and KEGG analyses. **(C-D)** GSEA analyses

model were established and corresponding prognostic predictive capacity was verified through ROC curves and regression analyses. According to the prognostic nomogram, the 3 - year survival rate of HCC patients could be predicted accurately. Besides, we found that this prognostic model could also distinguish patients with different therapeutic responses of Sorafenib, TACE, and immunotherapy according to the risk score of patients. Moreover, we explored the potential effective chemotherapeutic drugs of patients with high prognostic risks, which might provide a new method for therapeutic choice of HCC patients.

4 GMAGs (RRM1, RRM2, G6PD, and GPX7) with independent prognostic value were identified to establish our prognostic model. Some genes have been demonstrated to play essential roles in carcinogenesis or development of malignancies. Wang et al. [22] have found that the knockdown of RRM1 or G6PD could inhibit the proliferation of Hep3B cell line. RRM2 was demonstrated

to decrease intracellular reactive oxygen species (ROS) levels and inhibit ferroptosis in HCC [23, 24]. One study found that down-regulation of RRM2 could suppress proliferation, invasion, and metastasis of HCC cells [25]. In another study, to target the RRM2 could inhibit the DNA damage response and improve apoptosis in atypical teratoid rhabdoid tumor [26]. Besides, RRM2 was illustrated to stabilize the expression of ANXA1 to regulate prostate cancer progression and chemoresistance [27]. RRM1 and RRM2 had been illustrated to play complex roles in glutamine metabolism [28, 29]. G6PD is an important enzyme in the procedure of glycometabolism and tricarboxylic acid cycle. The lack of G6PD could lead to anemia or favism [30]. It has been demonstrated that suppressing the expression of G6PD could inhibit the growth of HCC [31]. G6PD was demonstrated to be correlated with glutamine metabolism. For instance, in melanoma cells, inhibition of G6PD could promote oxidative stress and glutaminolysis [32]. GPX7 is a kind of glutathione

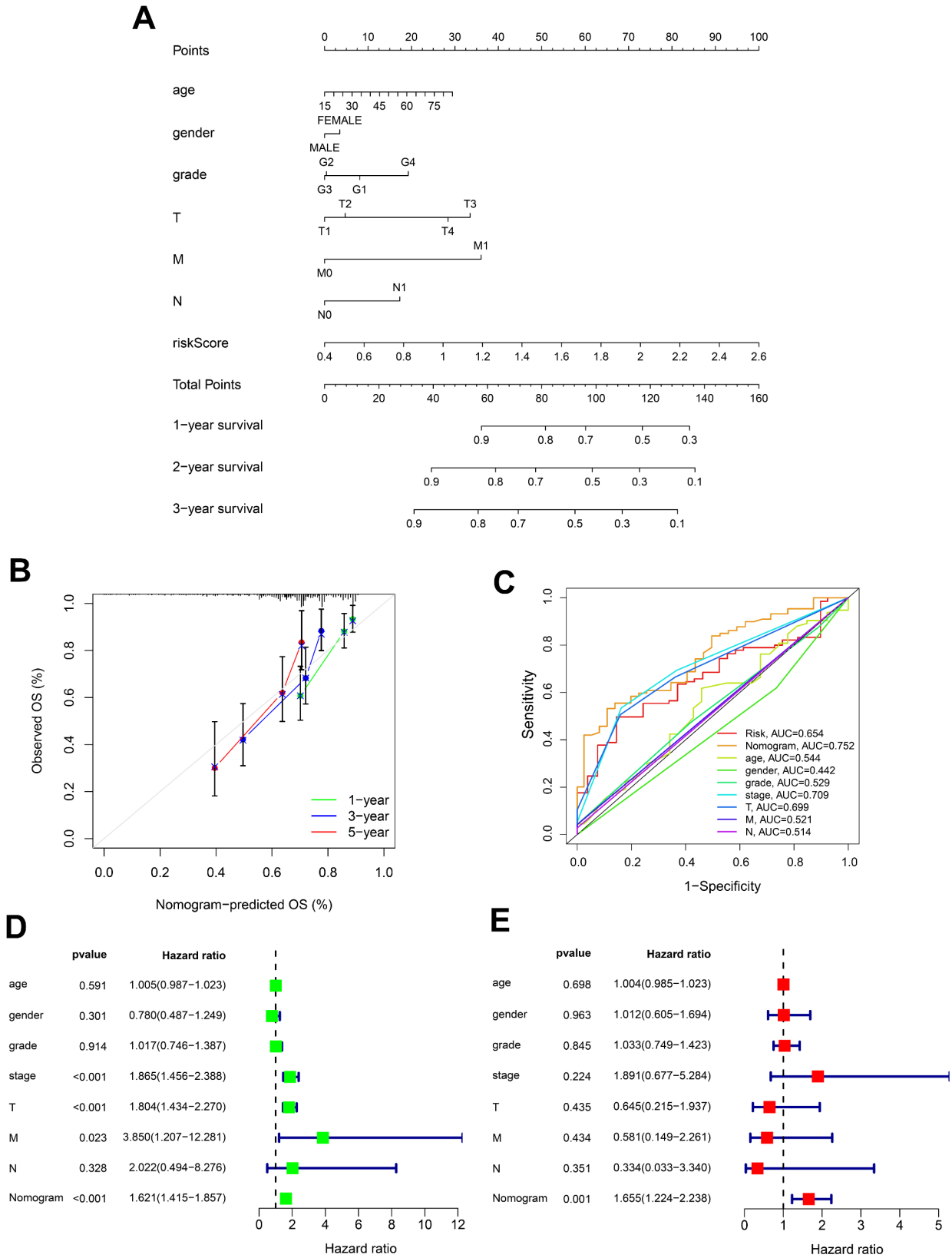


**Fig. 5** Establishment of the prognostic nomogram. **(A)** The prognostic nomogram to predict HCC patients' prognosis based on the prognostic model. **(B)** The corresponding calibration plot to show a strong prognostic predictive capacity of nomogram. **(C)** The multifactorial ROC curves to show the prognostic predictive value of this nomogram. **(D-E)** The results of univariate and multivariate Cox regression analyses to show an independent prognostic value of the nomogram

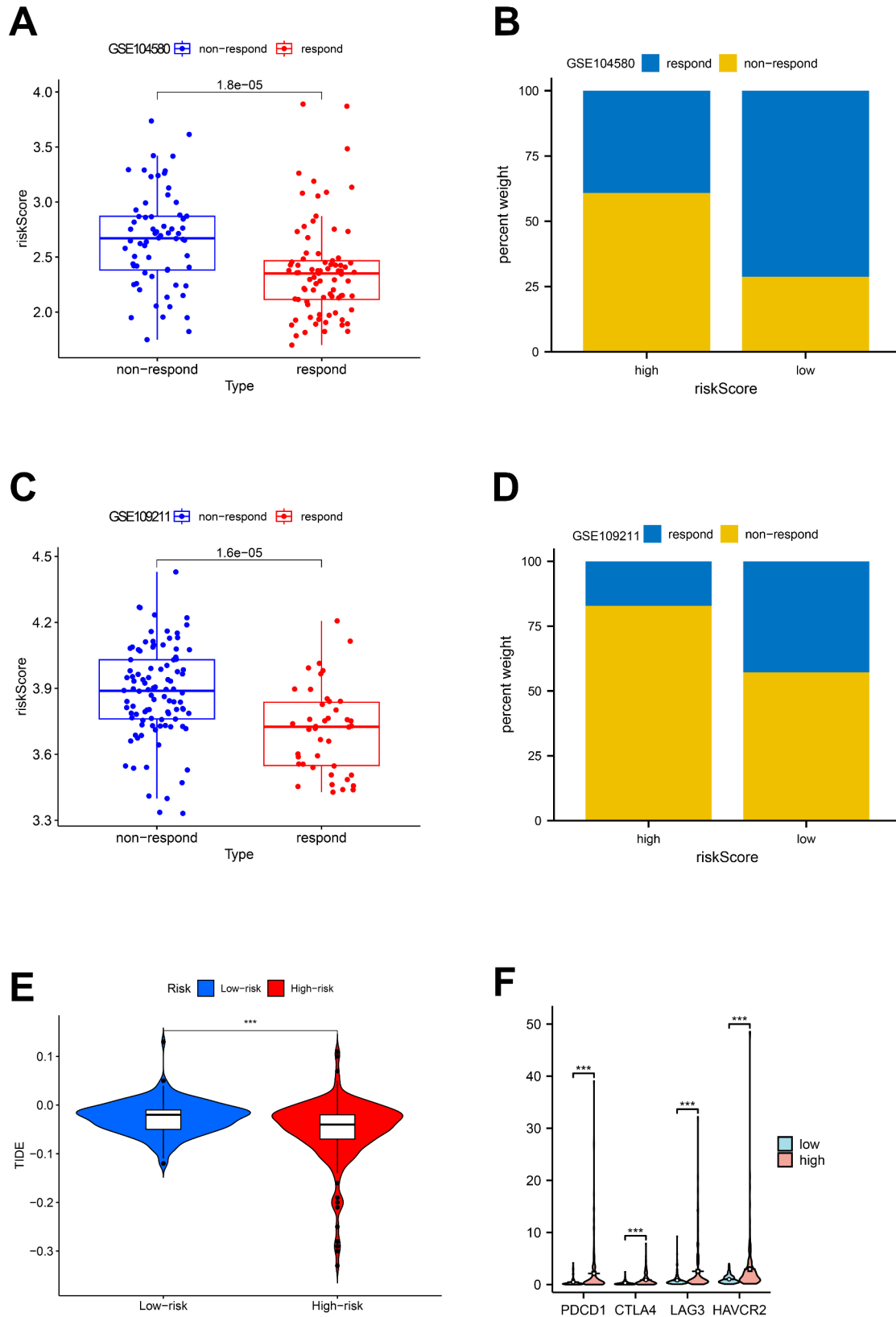


**Fig. 6** Assessment of the ability to predict therapeutic responses. **(A-B)** The results to show different responses to TACE between patients with different prognostic risks. **(C-D)** The results to show different responses to sorafenib between patients with different prognostic risks. **(E)** The result to show the TIDE scores of patients with different prognostic risks. **(F)** The expression of 4 common immune checkpoint genes between patients with different prognostic risks

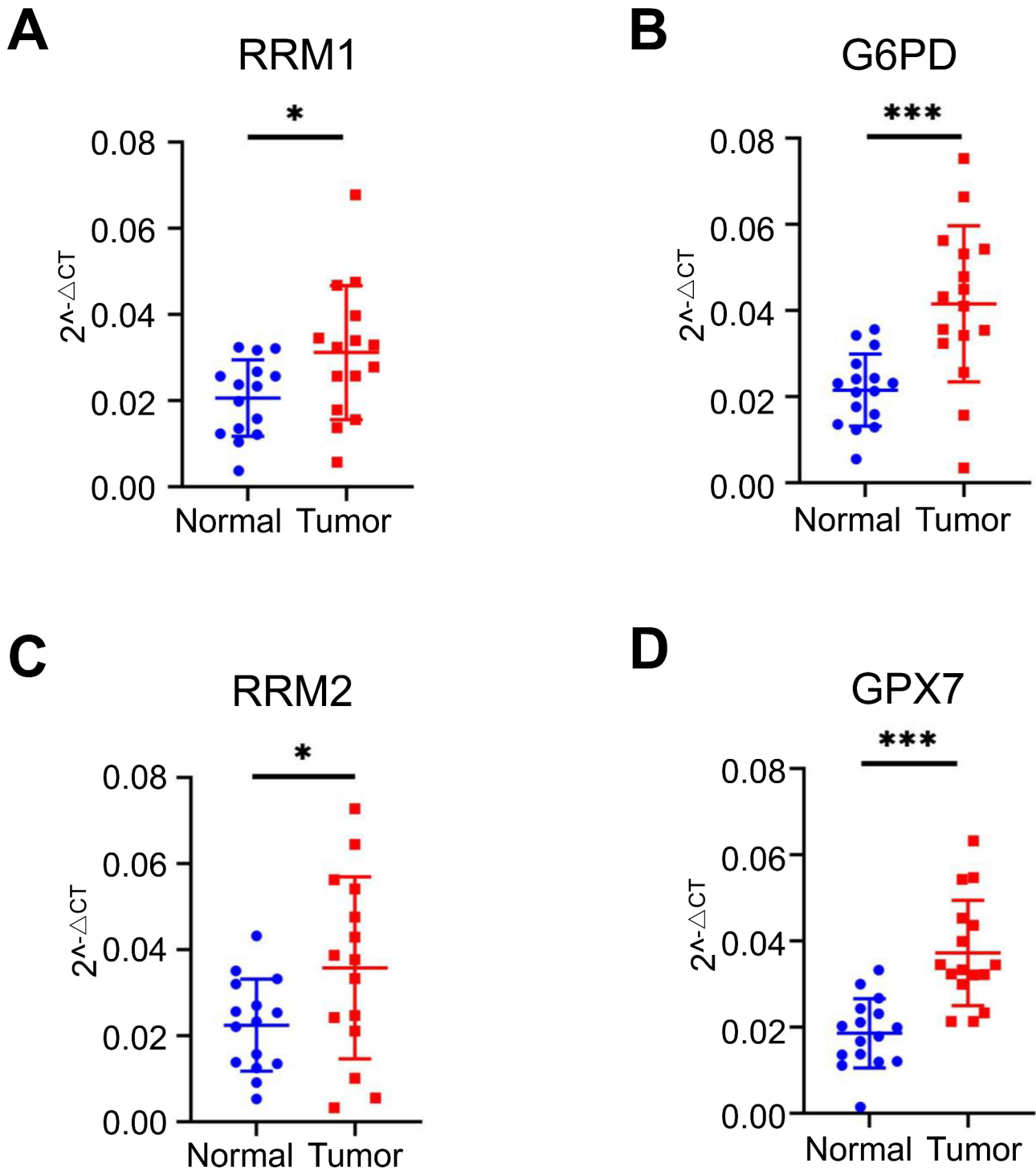


**Fig. 7** The results of qRT-PCR to show the expression levels of 4 DEARGs in clinical samples from HCC patients. (A) RRM1. (B) G6PD. (C) RRM2. (D) GPX7

peroxidase, which might be correlated with oxidative stress and interact with GSH [33]. Guerriero et al. [34] have found that the expression of GPX7 in HCC samples was higher than in cirrhosis tissues, which hinted a potential oncogenic role of GPX7 in HCC. Additionally, GPX7 could also improve the proliferation and inhibit

the apoptosis of human papillary thyroid carcinoma [35]. The expression level of 4 genes in HCC samples were investigated via qRT-PCR, and the results showed that all 4 genes have a higher expression in HCC samples than in normal samples. All these researches revealed that our prognostic model might be closely related with HCC.

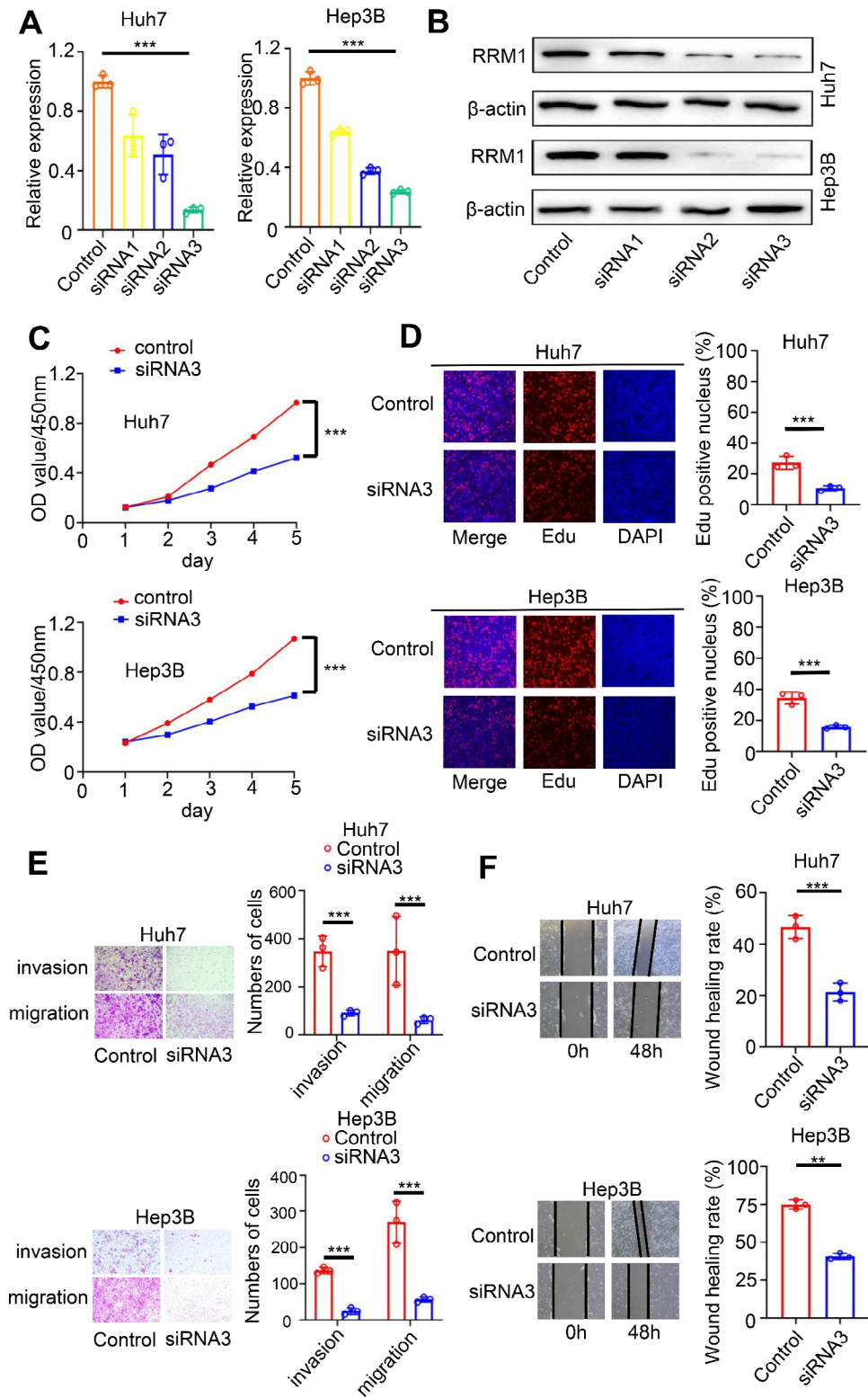


**Fig. 8** The suppression of RRM1 inhibit HCC proliferation, invasion, and migration in vitro. **(A)** Efficiency of RRM1 siRNA transfection in Huh7 and Hep3B cell lines were demonstrated by qRT-PCR. **(B)** Efficiency of RRM1 siRNA transfection in Huh7 and Hep3B cell lines were demonstrated by WB. **(C)** CCK8 assay was utilized to explore the effect of RRM1 on cellular proliferation. **(D)** Edu assay demonstrated the inhibition of RRM1 could suppress the proliferation. **(E)** Transwell assays illustrated the reduction of RRM1 inhibit invasion and migration. **(F)** Wound healing assay was used to evaluate the association between RRM1 and cellular migration

In this research, we investigated the function of gene RRM1 and choose HCC cell lines to explore the oncogenic role of RRM1 in vitro. All results showed that the knockdown of RRM1 could suppress the proliferation, invasion, and migration of Huh7 and Hep3B cells. According to our results, RRM1 might be a potential target for HCC treatment in the future. However, there are some shortcomings in our study. Due to the lack of data in large samples, we could not validate the prognostic capacity of prognostic model more precisely. Besides, more experiments about glutamine metabolism could be executed to explore the mechanism of these genes in HCC, which might indicate new direction for the diagnosis or treatment of HCC.

#### Abbreviations

HCC	Hepatocellular carcinoma
GSH	Glutathione
GMAGs	Glutamine metabolism associated-genes
TCGA	The Cancer Genome Atlas
ICGC	International Cancer Genome Consortium
GEO	Gene Expression Omnibus
GSEA	Gene Set Enrichment Analysis
TACE	Transhepatic arterial chemotherapy and embolization
DEGMAGs	Differentially expressed glutamine metabolism associated-genes
LASSO	Least absolute shrinkage and selection operator
K–M	Kaplan–Meier
ROC	Receiver operating characteristic
DEGs	Differentially expressed genes
KEGG	Kyoto Encyclopedia of Genes and Genomes
GO	Gene Ontology
GSEA	Gene Set Variation Analysis
TIDE	Tumor Immune Dysfunction and Exclusion
qRT-PCR	Quantitative real-time PCR
TBST	Tris-buffered saline-Tween
CCK8	Cell-Counting-Kit-8
ROS	Reactive oxygen species

#### Supplementary Information

The online version contains supplementary material available at <https://doi.org/10.1186/s13062-024-00567-x>.

Supplementary Material 1

Supplementary Material 2

#### Acknowledgements

All authors showed the thanks to Yahuan Xie (College of Education Science, Guangxi Minzu University, Nanning, Guangxi Zhuang Autonomous Region, China) for the help of data acquiring.

#### Author contributions

HX and CX designed this research. Cellular molecular experiments were accomplished by CZ and CX. HP and HX accomplished the data acquisition and the analysis by Perl language. CX and HX accomplished all the bioinformatic analyses of R language. HX, LF drew and accomplished the manuscript. WC provided the fund to accomplish this study. CX, CZ and WC were responsible for this research.

#### Funding

No application.

#### Data availability

No datasets were generated or analysed during the current study.

#### Declarations

##### Ethical approval

This research was approved by the Ethics Committee of Dalian medical university.

##### Competing interests

The authors declare no competing interests.

Received: 1 October 2024 / Accepted: 11 November 2024

Published online: 20 November 2024

#### References

1. Bray F, Laversanne M, Sung H, Ferlay J, Siegel RL, Soerjomataram I, et al. Global cancer statistics 2022: GLOBOCAN estimates of incidence and mortality worldwide for 36 cancers in 185 countries. *Cancer J Clin*. 2024;74(3):229–63.
2. Maki H, Hasegawa K. Advances in the surgical treatment of liver cancer. *Biosci Trends*. 2022;16(3):178–88.
3. Sun HC, Zhou J, Wang Z, Liu X, Xie Q, Jia W, et al. Chinese expert consensus on conversion therapy for hepatocellular carcinoma (2021 edition). *Hepatobiliary Surg Nutr*. 2022;11(2):227–52.
4. Llovet JM, Bru C, Bruix J. Prognosis of hepatocellular carcinoma: the BCLC staging classification. *Semin Liver Dis*. 1999;19(3):329–38.
5. Llovet JM, Pinyol R, Yarchoan M, Singal AG, Marron TU, Schwartz M, et al. Adjuvant and neoadjuvant immunotherapies in hepatocellular carcinoma. *Nat Reviews Clin Oncol*. 2024;21(4):294–311.
6. Ni R, Li Z, Li L, Peng D, Ming Y, Li L, et al. Rethinking glutamine metabolism and the regulation of glutamine addiction by oncogenes in cancer. *Front Oncol*. 2023;13:1143798.
7. Ye Y, Yu B, Wang H, Yi F. Glutamine metabolic reprogramming in hepatocellular carcinoma. *Front Mol Biosci*. 2023;10:1242059.
8. Kodama M, Nakayama KI. A second Warburg-like effect in cancer metabolism: the metabolic shift of glutamine-derived nitrogen: a shift in glutamine-derived nitrogen metabolism from glutaminolysis to de novo nucleotide biosynthesis contributes to malignant evolution of cancer. *BioEssays: News Reviews Mol Cell Dev Biology*. 2020;42(12):e2000169.
9. Zhang D, Hua Z, Li Z. The role of glutamate and glutamine metabolism and related transporters in nerve cells. *CNS Neurosci Ther*. 2024;30(2):e14617.
10. Yang L, Venneti S, Nagrath D. Glutaminolysis. A Hallmark of Cancer Metabolism. *Annu Rev Biomed Eng*. 2017;19:163–94.
11. Li Y, Li B, Xu Y, Qian L, Xu T, Meng G, et al. GOT2 silencing promotes reprogramming of glutamine metabolism and Sensitizes Hepatocellular Carcinoma to glutaminase inhibitors. *Cancer Res*. 2022;82(18):3223–35.
12. Shao M, Tao Q, Xu Y, Xu Q, Shu Y, Chen Y, et al. Glutamine synthetase-negative hepatocellular carcinoma has better prognosis and response to sorafenib treatment after hepatectomy. *Chin Med J*. 2023;136(17):2066–76.
13. Zeng Y, Jiang H, Zhang X, Xu J, Wu X, Xu Q, et al. Canagliflozin reduces chemoresistance in hepatocellular carcinoma through PKM2-c-Myc complex-mediated glutamine starvation. *Free Radic Biol Med*. 2023;208:571–86.
14. Tomczak K, Czerwińska P, Wiznerowicz M. The Cancer Genome Atlas (TCGA): an immeasurable source of knowledge. *Contemp Oncol (Poznan Poland)*. 2015;19(1a):A68–77.
15. Hudson TJ, Anderson W, Artez A, Barker AD, Bell C, Bernabé RR, et al. International network of cancer genome projects. *Nature*. 2010;464(7291):993–8.
16. Barrett T, Wilhite SE, Ledoux P, Evangelista C, Kim IF, Tomashevsky M, et al. NCBI GEO: archive for functional genomics data sets—update. *Nucleic Acids Res*. 2013;41(Database issue):D991–5.
17. Jiang J, Hu Y, Fang D, Luo J. Glutamine synthetase and hepatocellular carcinoma. *Clin Res Hepatol Gastroenterol*. 2023;47(10):102248.
18. Wu J, Xue R, Jiang RT, Meng QH. Characterization of metabolic landscape in hepatocellular carcinoma. *World J Gastrointest Oncol*. 2021;13(9):1144–56.
19. Kaur R, Kanthaje S, Taneja S, Dhiman RK, Chakraborti A. miR-23b-3p modulating Cytoprotective Autophagy and glutamine addiction in Sorafenib resistant HepG2, a Hepatocellular Carcinoma Cell line. *Genes*. 2022;13(8).
20. Wei D, Chen D, Mou H, Chakraborty S, Wei B, Tan L, et al. Targeting glutamine metabolism with a Novel Na<sup>+</sup>/K<sup>+</sup>-ATPase inhibitor RX108 in Hepatocellular Carcinoma. *Mol Cancer Ther*. 2023;22(6):693–705.
21. Zhao Y, Wang Y, Miao Z, Liu Y, Yang Q. c-Myc protects hepatocellular carcinoma cell from ferroptosis induced by glutamine deprivation via upregulating GOT1 and Nrf2. *Mol Biol Rep*. 2023;50(8):6627–41.

22. Wang Z, Fu Y, Xia A, Chen C, Qu J, Xu G, et al. Prognostic and predictive role of a metabolic rate-limiting enzyme signature in hepatocellular carcinoma. *Cell Prolif*. 2021;54(10):e13117.
23. Zhang X, Qi M, Huo K, Cai B, Zhang J, Tian Y, et al. Celastrol induces ferroptosis by suppressing RRM2 in hepatocellular carcinoma. *Heliyon*. 2024;10(13):e33936.
24. Chen B, Jin T, Fu Z, Li H, Yang J, Liu Y, et al. Non-thermal plasma-treated melatonin inhibits the biological activity of HCC cells by increasing intracellular ROS levels and reducing RRM2 expression. *Heliyon*. 2023;9(5):e15992.
25. Peng S, Yi L, Liao L, Bin Y, Qu W, Hu H. Circ\_0008285 knockdown represses tumor development by miR-384/RRM2 axis in hepatocellular carcinoma. *Ann Hepatol*. 2022;27(6):100743.
26. Giang LH, Wu KS, Lee WC, Chu SS, Do AD, Changou CA, et al. Targeting of RRM2 suppresses DNA damage response and activates apoptosis in atypical teratoid rhabdoid tumor. *J Experimental Clin cancer Research: CR*. 2023;42(1):346.
27. Cheng B, Li L, Wu Y, Luo T, Tang C, Wang Q, et al. The key cellular senescence related molecule RRM2 regulates prostate cancer progression and resistance to docetaxel treatment. *Cell Bioscience*. 2023;13(1):211.
28. Kuwasako K, Takahashi M, Tochio N, Abe C, Tsuda K, Inoue M, et al. Solution structure of the second RNA recognition motif (RRM) domain of murine T cell intracellular antigen-1 (TIA-1) and its RNA recognition mode. *Biochemistry*. 2008;47(24):6437–50.
29. Dye BT, Patton JG. An RNA recognition motif (RRM) is required for the localization of PTB-associated splicing factor (PSF) to subnuclear speckles. *Exp Cell Res*. 2001;263(1):131–44.
30. Beretta A, Manuelli M, Cena H. Favism: clinical features at different ages. *Nutrients*. 2023;15(2).
31. Wu Q, Ge XL, Geng ZK, Wu H, Yang JY, Cao SR, et al. HuaChanSu suppresses the growth of hepatocellular carcinoma cells by interfering with pentose phosphate pathway through down-regulation of G6PD enzyme activity and expression. *Heliyon*. 2024;10(3):e25144.
32. Aurora AB, Khivansara V, Leach A, Gill JG, Martin-Sandoval M, Yang C et al. Loss of glucose 6-phosphate dehydrogenase function increases oxidative stress and glutaminolysis in metastasizing melanoma cells. *Proc Natl Acad Sci USA*. 2022;119(6).
33. Chen Yi, Wei PC, Hsu JL, Su FY, Lee WH. NPGPx (GPx7): a novel oxidative stress sensor/transmitter with multiple roles in redox homeostasis. *Am J Translational Res*. 2016;8(4):1626–40.
34. Guerriero E, Capone F, Accardo M, Sorice A, Costantini M, Colonna G, et al. GPX4 and GPX7 over-expression in human hepatocellular carcinoma tissues. *Eur J Histochemistry: EJM*. 2015;59(4):2540.
35. Liu LD, Zhang YN, Wang LF. GPX7 promotes the growth of human papillary thyroid carcinoma via enhancement of cell proliferation and inhibition of cell apoptosis. *Translational cancer Res*. 2019;8(7):2570–80.

### Publisher's note

Springer Nature remains neutral with regard to jurisdictional claims in published maps and institutional affiliations.